Indian Journal of Pure & Applied Physics
Vol. 63, June 2025, pp. 479-487
DOI: 10.56042/ijpap.v63i6.13465

Contribution of Tensor Forces and Exchange Term for (^{3}He, t) Charge Exchange Reactions on Different Mass Targets

Ankita & Pardeep Singh*

Department of Physics, Deenbandhu Chhotu Ram University of Science and Technology, Murthal, Sonipat 131 039, India

Received: 30 August 2024; accepted: 21 May 2025

The angular distribution and unit cross-section for (^{3}He, t) charge exchange reactions at 140 MeV/nucleon on ^{13}C, ^{26}Mg, ^{58}Ni, and ^{120}Sn targets have been computed by employing the distorted wave impulse approximation. Particularly, the contribution of tensor forces and knock-on exchange term have been estimated and the substantial quantitative variations in the cross-section have been found which in turn brings the predications closure to the experimental results.

Keywords: Gamow-Teller transitions, Charge exchange reaction, Tensor forces, Distorted wave impulse approximation, Angular distribution

1 Introduction

In nuclear physics the charge exchange reactions (CERs) are widely used to explore the specifics of the reaction dynamics and structure of atomic nuclei. The investigation of charge exchange reactions has a long history, predating the formulation of modern atomic structure theories with the discovery of the first charge exchange process, beta decay. During past decade, the development of charged particle accelerators has made it possible to study nuclear processes, particularly charge exchange reactions, in more detail, bringing up new perspectives in this field. In these reactions, a particle like proton or neutron, is being transferred from one nuclear state to another retaining certain quantum numbers (orbital (L), spin (S) angular momentum and isospin (T)). Charge exchange reactions have also been used to explore the various aspects pertaining to nuclear astrophysics including electron capture, beta-decay, neutrino interactions and nuclear energy generation[1-3]. In addition, these reactions provide significant insights into the study of giant resonances as well as spin-isospin response in nuclei at both low and high energies[4-9].

Depending on the particles involved, charge exchange reactions have been executed through a variety of channels, including (p, n)/ (^{3}He, t), (n, p)/ (t, ^{3}He) and (d, ^{2}He). Proton and neutron beams have historically been used to study charge exchange reactions extensively, leading to the important advances in nuclear physics. Nevertheless, charge exchange reactions involving composite particles like ^{3}He and ^{3}H$_1$ have also gained much popularity in recent years. Specifically, the use of the (^{3}He, t) charge-exchange reaction (CER), improve energy resolution (upto 20 keV) and permits an accurate extraction of GT strength and present interesting facts for expanding our understanding of nuclear structure[10-12]. These reactions involve the interaction between ^{3}He nucleus (composed of two protons and one neutron) and a target nucleus, leading to the exchange of charge and energy. In these reactions, a proton from the projectile ^{3}He is transferred to the target nucleus and ^{3}He nucleus absorbs a neutron. As a result, the absorbed neutron and transferred proton undergo self-reconfiguration, resulting in the production of the final reaction products and a same process followed by β^- -decay as shown in Fig. 1.

Furthermore, charge exchange reactions also reveal important details regarding the strength of different transitions, such as the Gamow-Teller (GT), Fermi (F), spin dipole and spin quadrupole transitions. Out of which GT transitions (with $\Delta S=1$, $\Delta L=0$ and $\Delta T=1$) fascinates significant attractions because they are used to extract weak transition strengths in excitation-energy regions, which usually remains inaccessible during beta-decay. Therefore, the charge exchange reaction leading to the Gamow-Teller transitions have been investigated for several targets and a phenomenological correlation between the GT cross-section and the target mass number has been established. This relationship serves as a valuable

*Corresponding author: (E-mail: panghal005@gmail.com)

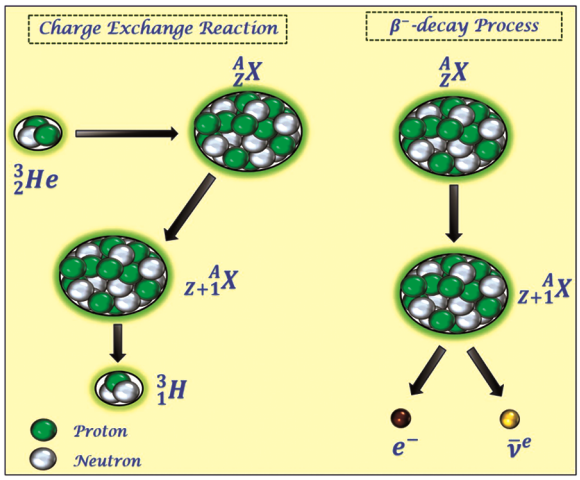

Fig. 1 — (color online) Illustration of charge exchange reaction (^{3}He, t) and β^- decay process

means to validate the estimated unit cross-sections in cases where corresponding experimental results are unavailable[13,14].

Also, previous studies explored complex valence-space effective operators for the Gamow-Teller (GT) transition in nuclei near the driplines, using many-body perturbation theory within the complex-energy Berggren basis and the EM1.8/2.0 chiral effective field theory interaction[15]. The findings highlight significant isospin asymmetry in mirror nuclei ^{22}Si - ^{22}O and their daughters ^{22}Al - ^{22}F, underscoring the importance of continuum coupling in accurately describing GT transitions and mirror energy differences. Understanding of evolution of nuclear shells is crucial for refining nuclear models and interpreting experimental data of charge exchange reactions. Recent studies shows that tensor forces, due to σ and π meson exchanges, cause systematic shifts in single-particle energies and impact shell structures from the p shell to superheavy elements[16]. These effects align with chiral perturbation theory, highlighting the significant role of tensor force in shell evolution. However, more work is needed to explore its interaction with central forces and its broader implications on nuclear structure. Also, the role of tensor correlations in nuclear excitations has been a key focus in recent studies which aimed to refine the Skyrme interaction parameters and identifies specific parameter sets that align well with experimental data[17]. Further, by C. L. Bai Zhang *et al*., the analysis of Gamow-Teller (GT) and charge-exchange spin-dipole (SD) excitations in ^{90}Zr and ^{208}Pb has demonstrated that tensor terms significantly influence the excitation energies[18]. The results highlight that tensor interactions lead to a downward shift of the main GT peaks by approximately 2 MeV and shift about 10% of the non-energy weighted sum rule to higher excitation energies and uniquely impact SD excitations depending on the multipole states. In a recent analysis Yang et al., highlights the significance of 2p-2h correlation and tensor interactions in refining $\beta-$ decay models for closed shells nuclei. The study demonstrates that the SSRPA model, which includes both 1p-1h and 2p-2h configurations, allowing for a more accurate representation of Gamow-Teller (GT) strength distributions and the inclusion of tensor force leads to significantly improved predictions[19]. The work also highlights the crucial role of tensor interactions in shaping GT and SD excitations. Although, in most of previous analysis of charge exchange reactions, the theoretical calculations have been estimated with approximate consideration of knock-on exchange effects. Also, the tensor force effects have been ignored in these calculations[20]. However, the importance of inclusion of contributions of exactly calculated exchange terms and tensor forces in the analysis of charge exchange reactions data have been signatured by many authors[21,22]. Therefore, it is essential to pay close attention to estimate the contribution of the direct and exchange term along with the inclusion of tensor forces in order to derive clearer and more accurate information from these reactions. With this aim, we present the results of our calculations for charge exchange reactions produced by ^{3}He projectiles at a beam energy of 140 MeV/nucleon on various targets from low to heavy mass nuclei for Gamow-Teller transitions. Particularly, the unit cross-sections and angular distributions have been estimated.

2 Theoretical Formalism

The distorted wave impulse approximation (DWIA) framework has been used, which is a reliable and successful theoretical tool for examining the charge exchange reactions at intermediate energies (around 100 MeV/nucleon). The DWIA technique accounts for both the direct and exchange contributions to the scattering processes as well as the distortion of the incident and outgoing waves caused by the nuclear potential. Here, we have employed computer code DCP-2 (which is based on DCP-1[22]) for calculations. The knock-on exchange effects (previously either ignored or calculated approximately) are precisely examined by the fully antisymmetric DCP-2 code by employing the multipole expansion approach. In DCP-1, one body transition

densities (OBTDs) are assumed to be unity, however, in DCP-2 explicitly includes OBTDs implies as pure 1p–1h configurations, present a more accurate calculations of the nuclear transitions. The formalism and calculation details pertaining to DCP-2 have been elaborated in details in references[23-25]. However, for the ready reference of the readers a brief outline of the formulism is discussed here.

In this approach, the following expression has been used to estimate the differential cross-section for A(a, b)B type charge exchange reaction,

$$\frac{d\sigma}{d\Omega} = \frac{\mu_a \mu_b}{(2\pi\hbar^2)^2}\frac{k_b}{k_a} \times \left|\sum_{i=D,E}\sum_{k,l_1 t_1} \alpha_{j_t s_t \nu_1}^{t_1 s_1 l_1 k l_t} T_i^{t_1 s_1 l_1 k l_t m_{l_t}}\right|^2 \quad \ldots (1)$$

Here, the reduced reactant mass in entrance and outgoing channels is represented by μ_a *and* μ_b respectively. k_a and k_b give the wave numbers in the incident and exit channels respectively. The expansion coefficient $\alpha_{j_t s_t \nu_1}^{t_1 s_1 l_1 k l_t}$ can be expressed in terms of the Racah coefficient (W), exhibiting the spectroscopic amplitude for projectile spin-isospin wave function and the recoupling of angular momenta and may be expressed as

$$\alpha_{j_t s_t \nu_1}^{t_1 s_1 l_2 k l_t} = W(s_t l_t s_t l_1; j_t k)\hat{s}_t^{-1} t_1^{-1} < b \| [c^{\dagger} c]_{s_1 t_1 \tilde{\nu}_1} \| a > \quad \ldots (2)$$

with $\hat{s} = \sqrt{2s+1}$. $T_i^{t_1 s_1 l_1 k l_t m_{l_t}}$ is the transition amplitude required to estimate the differential cross-section with subscript i stands for the direct $(i = D)$ and exchange $(i = E)$ terms contributions and may be further expressed in terms of overlap radial integrals given as:

$$T_i^{t_1 s_1 l_1 k l_t m_{l_t}} = \frac{(4\pi)^{3/2}}{k_a k_b}\sum_{l_a l_b} i^{l_a - l_b + \pi}\hat{l}_a (l_a 0 l_t m_{l_t} | l_b m_{l_t}) \times O_{t_1 s_1 l_1 k l_t, l_a l_b}^{i} Y_{l_b m_{l_t}}(\hat{k}_b) \quad \ldots (3)$$

Now, respectively the direct and exchange overlap integrals are defined as

$$O_{t_1 s_1 l_1 k l_t, l_a l_b}^{D} = \frac{1}{4\pi}\hat{l}_a \hat{l}_t \hat{l}_b^{-1}(l_a 0 l_t 0 | l_b 0) \times \int dr_a \, \chi_{l_b}(r_a) f_{t_1 s_1 l_1 k l_t}^{D}(r_a)\chi_{l_a}(r_a) \quad \ldots (4)$$

and

$$O_{t_1 s_1 l_1 k l_t, l_a l_b}^{E} = J \int dr_b \int dr_a \, r_b r_a \chi_{l_b}(r_a) \times f_{t_1 s_1 l_1 k l_t, l_a l_b}^{E}(r_b, r_a)\chi_{l_b}(r_b), \quad \ldots (5)$$

Here, $\chi_{l_a}(r_a)$ and $\chi_{l_b}(r_b)$ are the partial distorted waves in the incident and exit channels respectively. J is the Jacobian associated with the transformation of integral coordinate from $\vec{r}_2$ to $\vec{r}_a$ and $\vec{r}_b$. The form factor appeared in Eqs (4) and (5) for direct and exchange terms are given by f^D and f^E and further expressed as

$$f_{t_1 s_1 l_1 k l_t}^{D}(r_a) = \iota^{-\pi}(-)^{l_1}\hat{l}_t^{-1}\int r^2 dr \times V_{t_1 s_1 k}^{D}(r)\int r_1^2 dr_1 \rho_{P,kl_t l_1}^{D}(r_a, r_1, r)\rho_{T,l_1}^{D}(r_1) \quad \ldots (6)$$

and

$$f_{t_1 s_1 l_1 k l_t, l_a l_b}^{E}(r_b, r_a) = J 4\pi m_a^k \sum_{\lambda_a \lambda_b l_a l_\beta}\left[\frac{(2k+1)!}{(2\lambda_a+1)!(2\lambda_b+1)!}\right]^{\frac{1}{2}} \times \delta_{\lambda_a+\lambda_b,k}(-r_a)^{\lambda_a}(r_b)^{\lambda_b} X(l_\alpha \lambda_a l_a, l_\beta \lambda_b l_b; l_t k l_t) \times d_{l_\alpha \lambda_a l_a} d_{l_\beta \lambda_b l_b} c_{t_1 s_1 l_1 k, l_\alpha l_\beta}(r_b, r_a) \quad \ldots (7)$$

respectively. The Fano coefficient, denoted as X, characterizes the distribution of angular momentum values in a spectroscopic transition. The code DCP-2 employs the multipole expansion method, wherein both the projectile and target transition densities are expanded into multiple terms with different polarities, represented by λ. In Eq 7, the appeared d and c-factors are defined below,

$$d_{l_\alpha \lambda_a l_a} = \frac{1}{\sqrt{4\pi}}\frac{\hat{l}_\alpha \hat{\lambda}_a}{l_a}(l_\alpha 0 \lambda_a 0 | l_a 0) = \frac{1}{\sqrt{4\pi}}\delta_{l_\alpha \lambda_a l_\alpha}$$

$$d_{l_\beta \lambda_b l_b} = \frac{1}{\sqrt{4\pi}}\frac{\hat{l}_\beta \hat{\lambda}_b}{l_b}(l_\beta 0 \lambda_b 0 | l_b 0) = \frac{1}{\sqrt{4\pi}}\delta_{l_b \lambda_b l_\beta}$$

and

$$c_{t_1 s_1 l_1 k, l_\alpha l_\beta}(r_b, r_a) = \frac{2\pi}{\hat{l}_1^2}\sum_{m_{l_1}} \hat{l}_\beta (l_\alpha m_{l_1} l_\beta 0 | l_1 m_{l_1}) \times \sum_{l\lambda} \hat{l}(l 0 \lambda m_{l_1} | l_1 m_{l_1}) \int d\mu \, G_{t_1 s_1 l_1 l\lambda}^{k}(r_b, r) \times Y_{\lambda m_{l_1}}(\theta', \pi) Y_{l_\alpha m_{l_1}}^{*}(\theta, 0)$$

with G-factor:

$$G_{t_1 s_1 l_1 l\lambda}^{k}(r_b, r) = \frac{1}{\sqrt{4\pi}} r^{-k} V_{t_1 s_1 k}^{E}(r)\sum_{\lambda_1 \lambda_2 l_c}(-)^{l}\hat{\lambda}_1 \hat{\lambda}_2 \times (\lambda_1 0 \lambda_2 0 | \lambda 0) W(\lambda_1 \lambda_2 l_1 l; \lambda l_c) \times \int r_1^2 dr_1 \rho_{P,\lambda_2 l l_c}^{E}(r_b, r_1, r)\rho_{T,\lambda_1 l_1 l_c}^{E}(r_1, r). \quad \ldots (8)$$

The fundamental reaction mechanism in this approach is to study the nucleon-nucleon (NN) effective interactions involving direct and exchange

components. Also, the effective interaction has a Yukawa-type radial dependence with local, central and tensor components with spin-spin and isospin-isospin interactions. The NN interaction potential (V), which is readily written as

$$V = \int dx_1 dx_2 dx_1' dx_2' \hat{\rho}_T(x_1, x_1') \hat{\rho}_P(x_2, x_2') \times v_{12}(x_1' x_2', x_1 x_2) \quad \ldots (9)$$

where, $x_i = (r_i, \sigma_i, \tau_i)$ stands for space, spin and iso-spin co-ordinate of i^{th} particle ($i = 1,2$) and x_i' co-ordinate denotes the x_i after the exchange of nucleons '1' and '2'. The interaction potential, expressed as $v_{12}(x_1' x_2', x_1 x_2) = x_1' x_2' V^D x_1 x_2 + (-)_l P^r \times x_1' x_2' V^E x_1 x_2$, with P^r as exchange operator, is a combination of direct and exchange part of the Love and Franey type effective interaction (V^i $(i = D)$ for direct and $(i = E)$ for exchange)[26,27]. The interaction potential (v_{12}) also include spin-orbit ($V^{LS}(r_{12})\vec{L} \cdot \vec{S}$) and tensor ($V^T(r_{12})\, \hat{S}_{12}$) terms respectively. Here, $\vec{L} \cdot \vec{S}$ and $\hat{S}_{12}$ are the common spin-orbit and tensor operators. The tensor operator can be written as $\hat{S}_{12} = 3(\hat{\sigma}_1 . \hat{r}\,)(\hat{\sigma}_2 . \hat{r}\,) - (\hat{\sigma}_1 . \hat{\sigma}_2\,) = \sum_q \sqrt{4\pi} \sqrt{\frac{2}{5}}\, Y_{2q}^* \hat{T}_{2q}$,

where $\hat{T}_{2q}$ is a second rank tensor operator. The $\hat{\rho}_T(x_1, x_1')$ and $\hat{\rho}_P(x_2, x_2')$ respectively accounts the non-local densities for target and projectile and can be expressed in terms of raising ($\hat{\Psi}^\dagger(x)$) and lowering ($\hat{\Psi}\,(x)$) operators of the nucleon field. The single-particle (hole) creation (annihilation) operator, $\hat{a}^\dagger_{j_p m_p \upsilon_p}\big(\hat{a}_{j_h m_h \upsilon_h}\big)$, with $\eta_{\upsilon_p}(\eta^*_{\upsilon_h})$ as the isospin part of the single-particle(hole) wave function $\phi_{j_p m_p}(\phi^*_{j_h m_h})$ and the raising and lowering operators are expressed as:

for target

$$\hat{\Psi}^\dagger_T(x_1) = \sum_{p,\upsilon_p} \hat{a}^\dagger_{j_p m_p \upsilon_p} \phi_{j_p m_p} \eta_{\upsilon_p}$$
$$\hat{\Psi}_T(x_1) = \sum_{h,\upsilon_h} \hat{a}_{j_h m_h \upsilon_h} \phi^*_{j_h m_h} \eta^*_{\upsilon_h} \quad \ldots (10)$$

and for projectile

$$\hat{\Psi}^\dagger_P(x_2) = \sum_{i\mu\upsilon} \hat{c}_i^\dagger \hat{c}_\mu^\dagger \hat{c}_\upsilon^\dagger \phi_i(\overrightarrow{r_2}) \xi_\mu(2) \eta_\upsilon(2)$$
$$\hat{\Psi}_P(x_2) = \sum_{i\mu\upsilon} \hat{c}_i \hat{c}_\mu \hat{c}_\upsilon \phi_i^*(\overrightarrow{r_2}) \xi_\mu^*(2) \eta_\upsilon^*(2) \quad \ldots (11)$$

Here, ϕ_i represents the spatial part of the projectile wave function, ξ_μ represents the spin part, η_υ represents the isospin part, and $\hat{c}^\dagger(\hat{c})$ represents the creation (annihilation) operator. Now using expression of Eqs (1) and (12) (Section 3.2) the differential cross-section and unit cross-section for various charge exchange reactions has been estimated and discussed in next sections.

3 Results and Discussion

The results obtained for charge exchange reactions involving ^{3}He as projectile on different mass targets at 140 MeV/nucleon energy have been presented in this section by employing distorted wave impulse approximation. Specifically, the contribution of the inclusion of exchange terms with and without tensor component has been estimated in the calculation of both unit cross-section and angular distribution. The optical model potential (OMP), transitions strength (B(GT)) and the effective nucleon-nucleon interaction are the inputs required for these calculations. Additionally, one-body transition densities (OBTDs) providing spatial distribution of nucleons in the initial and final nuclear states also required. OBTDs are also used to study the probability distributions of nucleons during nuclear transitions and provide essential information about the structure and dynamics of the nucleus. The many-body transition densities in the code are created by adding the OBTDs derived from microscopic calculations, such as shell-model calculations, as a weight factor for each one-particle one-hole excitation state. The algorithm operates in configuration space and Gaussian quadrature with a large number of integration points has been used to confirm correct convergence. In addition, the computer code used in this work enable us to select spectroscopic parameters in the computation of wave function of particle-hole states for both target and projectile systems. As a result, the many-body dynamics involved in composite particle scattering processes can be described more precisely. Effective nucleon-nucleon (NN) interaction, has been constructed by Love and Franey parameterization of the nucleon-nucleon t-matrix at an energy of 140 MeV/u derived from LAMPF version of SP84 amplitude[26-28]. The transition strength (B(GT)) and OMP parameters used in the calculations are taken from references[20,29,30] and are tabulated in Tables 1 and 2.

3.1 Angular Distribution

3.1.1 ^{13}C (0^+, g.s.) (^{3}He, t) ^{13}N (1^+, 15.1) Reaction

H. Fujimura *et al.* has examined the isobaric mirror relationship between ^{13}C and ^{13}N at bombarding

energies 150 MeV/nucleon. It is clearly recommended that the emission of protons originating from T = 3/2, $3/2^-$ states in ^{13}N at E_x = 15.06 MeV using ^{11}B (^{3}H, np)^{12}C reaction at low incident energies have provided crucial insights into configurations involving particles in sd-shell orbitals[29]. The study also highlights; the presence of specific configurations influences the excitation of Gamow-Teller (GT) and spin-dipole states.

Furthermore, this study connects the proton decay data from $1/2^-$ and $3/2^-$ states of ^{13}N to the 0^+ states in ^{12}C, providing insights into their coupling. The results challenge existing models and suggest further investigations. Therefore, in our analysis we have examine the results for ^{13}C (^{3}He, t) ^{13}N reactions at 140 MeV/nucleon in the framework of distorted-wave impulse approximation (DWIA) and the calculated differential cross- sections for 1^+ state at E_x= 15.1 of ^{13}C are presented in Fig. 2.

Figure 2 depicts the four different calculations along with the experimentally measured angular distribution taken from reference[29]. These calculations have been performed by using input parameters (B(GT) and optical model potentials (OMP) parameters) tabulated in Tables 1 and 2. The transition densities used has been calculated with the OXBASH code using p-sd model space with USD hamiltonian for ^{13}C nuclei[35]. Calculations performed without and with inclusion of exchange terms contribution are termed as Direct (D) and Total (D+E) respectively. Furthermore, the results shown by solid (red) and dashed dotted (green) lines are obtained by ignoring and with the inclusion of tensor forces along with exchange term respectively. While the dotted (black) and dashed (blue) lines are obtained by ignoring exchange terms but with and without inclusion of tensor forces respectively.

Due to inclusion of tensor forces contribution in direct as well as total (D+E) calculations, small change in the magnitude of differential cross-section has been observed. Here, we have found that the consideration of exchange terms with the direct terms decreases the cross-section in magnitude upto 21% and brings the magnitude towards experimental data. However, at small angles the magnitude of cross-section increases by 17% due to the inclusion of tensor forces in the calculation performed with direct as well as total (D+E) terms and take it away from the data.

To ascertain the observation found for ^{13}C (^{3}He, t) ^{13}N reaction here the same calculation for ^{26}Mg (^{3}He, t)^{26}Al reaction also has been performed and discussed in next subsection.

3.1.2 ^{26}Mg (0^+, g.s.) (^{3}He, t) ^{26}Al (1^+, 1.06) Reaction

R. G. T. Zegers *et al.* analyzed the (t,^{3}He) reaction at 115 MeV/nucleon energy and (^{3}He, t) reaction at

Table 1 — Initial and final states of various systems excited by reaction (^{3}He, t). B(GT) values are calculated by employing method given in references [32-34]

$Initial\ (J^\pi, E)$	$Final\ (J^\pi, E)$	$B(GT)$
$^{13}C(0^+, g.s.)$	$^{13}N(\frac{3^-}{2}, 15.1)$	0.23
$^{26}Mg(0^+, g.s.)$	$^{26}Al(1^+, 1.06)$	1.1
$^{58}Ni(0^+, g.s.)$	$^{58}Cu(1^+, g.s.)$	0.155
$^{120}Sn(0^+, g.s.)$	$^{120}Sb(1^+, g.s.)$	0.345

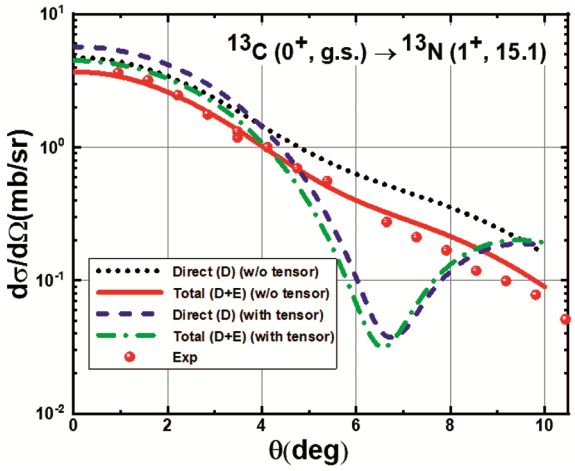

Fig. 2 — (Color online) The calculated differential cross-section for ^{3}He induced charge exchange reaction on ^{13}C target using DWIA at 140 MeV/nucleon. The dotted (black) and solid (red) line represents the direct and total (D+E) contribution without tensor forces effect respectively. The dashed (blue) and dash-dotted (green) line represents the direct and total (D+E) contribution with tensor forces effect respectively. The solid (red) circle represents the experimentally measured data

Table 2 — The optical potential parameters used in the calculations for incoming channel (^{3}He) are taken from the references[20,29,30]. while for outgoing channel (^{3}H) same parameters are used except potential depth which is modulated by multiplying with 0.85[31]

Target	$V_R(MeV)$	$r_R(fm)$	$a_R(fm)$	$W_i(MeV)$	$r_i(fm)$	$a_i(fm)$
^{13}C	19.10	1.55	0.70	36.0	0.94	0.86
^{26}Mg	27.3	1.36	0.87	85.9	0.46	1.12
^{58}Ni	35.16	1.32	0.84	44.43	1.021	1.018
^{120}Sn	31.02	1.36	0.81	45.10	1.044	1.055

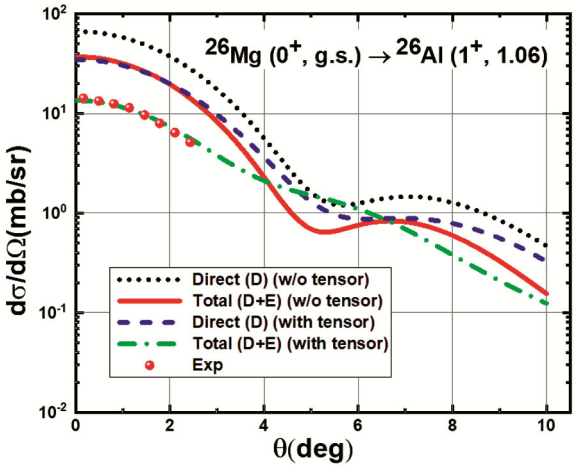

Fig. 3 — (Color online) Same as Fig. 2 but for ^{26}Mg (^{3}He, t)^{26}Al reaction

140 MeV/nucleon on ^{26}Mg and also highlights the importance of exact estimation of exchange effects[14]. Therefore, here we have analyzed the results of ^{26}Mg (^{3}He, t) ^{26}Al reactions at 140 MeV/nucleon. The differential cross-sections for 1^+ state at E_x= 1.06 for ^{26}Mg target have been computed and compared with the measured angular distribution data taken from reference[14]. Figure 3 also depicts four different calculations along with experimental data. The input parameters required for the calculations are presented in Table 1 and 2. Also the transition densities were calculated with the OXBASH code using sd model space with USD hamiltonian for ^{26}Mg targets[35]. It is clearly visible from Fig. 3 that the inclusion of tensor forces in both direct (D) and total (D+E) calculations to led significant change in the differential cross-section magnitude at small angles.

As we can observe that the calculated cross-section (for Direct (D)) overestimated the experimental data when exchange and tensor terms have been ignored. Although, when exchange term has been added with direct term (total (D+E) without tensor), the cross-section magnitude reduced up to 44% but still it fails to reproduce the experimental data. Furthermore, when tensor forces along with direct and total (D+E) contributions were included, the cross-section magnitude decreases upto 60% and brings it towards the experimental results.

3.1.3 ^{58}Ni (0$^+$, g.s.) (^{3}He, t) ^{58}Cu (1$^+$, g.s.) Reactions

In this sub-section, the calculated results for (^{3}He, t) reaction involving middle mass nuclei at 140 MeV/nucleon energy are discussed and analyzed.

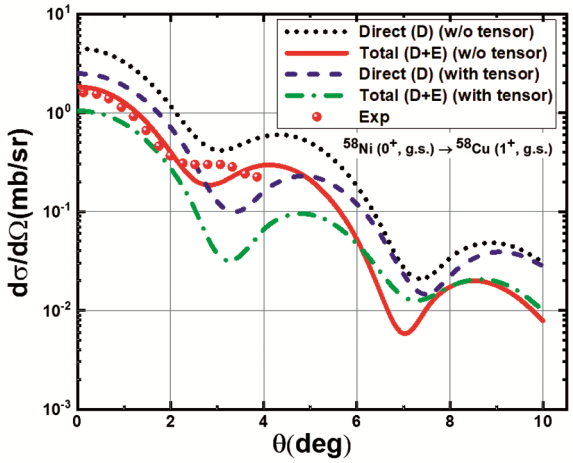

Fig. 4 — (Color online) Same as Fig. 2 but for ^{58}Ni (^{3}He, t)^{58}Cu reaction

Figure 4 depicts the calculated results of differential cross-section for ^{58}Ni (^{3}He, t) ^{58}Cu reaction for 1^+ ground states along with the measured experimental angular distributions taken from reference[20]. The input parameters used in the calculations are presented in Tables 1 and 2. The one-body transition densities used for Ni-isotopes were also calculated with the OXBASH code with pf-model space and the new effective GXPF1 interaction[36].

On examining Fig. 4, it is observed that the calculated differential cross-section corresponding to direct term overestimated the experimental data. However, on inclusion of exchange term the cross-section decreased upto 50% which in turn reduce the gap between predications and data.

The cross-section further reduced in magnitude (upto 45%) when tensor forces contribution has been included in the calculation of both direct (D) and total (D+E) at small angles. It is pertinent to mention here that due to incorporation of tensor forces contribution the predications move far to data.

3.1.4 ^{120}Sn (0$^+$, g.s.) (^{3}He, t) ^{120}Sb (1$^+$, g.s.) Reactions

In order to generalize the observations found in case of light and medium mass nuclei here we have performed the similar calculations for reaction involving heavy mass nuclei ^{120}Sb and obtained results are presented in Fig. 5. Input parameters, OMP and B(GT) are detailed in table 1 and 2 and the OBTD used for Sn-isotopes has been calculated by employing Sn-100nn model space with Sn100nn interaction which was derived by Brown et al. using G-matrix[37]. In Fig. 5, same as for other system discussed in previous subsections here, we have

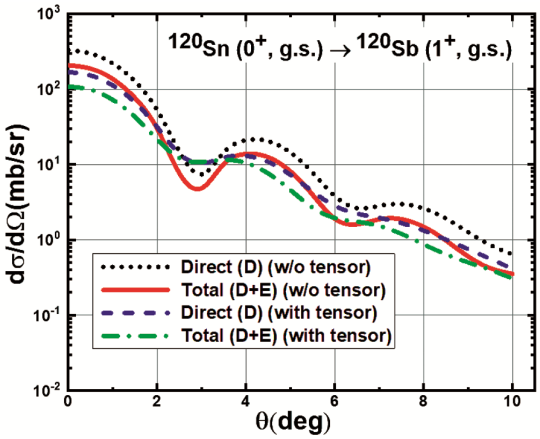

Fig. 5 — (Color online) Same as Fig. 2 but for ^{120}Sn (^{3}He, t) ^{120}Sb reaction

presented four different calculations for ^{120}Sn (^{3}He, t) ^{120}Sb reaction. The contribution of direct (D) and total (D+E) calculations by considering the tensor forces effects has been shown by dashed (blue) and dashed-dotted (green) lines respectively. While the dotted (black) and solid (red) lines represents the contribution of direct (D) and total (D+E) terms by ignoring tensor forces respectively.

It becomes clear that the consideration of tensor with direct and total components the cross-section is reduced at small angles. Particularly, with inclusion of exchange terms (total (D+E) without tensor), the differential cross-section magnitude decreased by 36%. Further, when tensor forces contribution in total (D+E) calculation has been included, the cross-section magnitude decreased upto 50%.

The results shown in Figs. 2-5 may be understand with the fact that the tensor component of the effective nucleon-nucleon interaction that mediates the charge-exchange reaction cause the interference between the ΔL=0 or 2 amplitudes since both contributes to the ΔJ=1 GT transition. The interference can be constructive as well as destructive and the behaviour of tensor component is found constructive in nature for ^{13}C (^{3}He, t) ^{13}N reaction. Although, for charge exchange reactions on ^{26}Mg, ^{58}Ni and ^{120}Sn target nuclei shows destructive interference behaviour. For further analysis of these reactions, we have also computed the unit cross-section and the results obtained are discussed in next section.

3.1.5 Unit Cross-Section and Contribution of Tensor Forces

The determination of unit cross-section $\hat{\sigma}_{GT}$ from charge-exchange (CE) reaction data is based on the relationship between GT transition strength and the differential cross section at zero momentum transfer

$$\frac{d\sigma}{d\Omega}(q \to 0) = \hat{\sigma}_{GT} B(GT) \quad \ldots (12)$$

Here, $\hat{\sigma}_{GT}$ denotes the unit cross-section for Gamow-Teller (GT) transitions measured at zero degrees and B(GT) is referred as the GT transitions strength[36,38,39]. The calculations of unit cross-section required B(GT) values (which were often acquired from β-decay studies), however if these values are not available, it becomes necessary to rely on theoretical calculations to determine the unit cross-section. Alternatively, one can also use empirical formulas, as discussed in reference[20]. However, it should be noted that the accuracy of empirical formulas is limited and theoretical calculations are often required to obtain more accurate estimates. In this subsection, the calculated results for unit cross-section and its variations over different target mass nuclei i.e., ^{13}C, ^{26}Mg, ^{58}Ni, and ^{120}Sn are discussed. Figure 6 depicts the four different calculations for each target along with the results obtained through empirical relation, $\hat{\sigma}_{GT,fit} = 109/A^{0.65}$, which is a power fit to the experimental results[14]. In Fig. 6 (a), respectively the up-triangle (green) and down-triangle (blue) shows direct and total (D+E) calculations without considering tensor forces. While solid (black) square and solid (red) circles are showing the results after consideration tensor forces in the calculation with direct and total (D+E) term respectively. The solid (black) line represents the unit cross-section obtained through empirical function. To assess the credibility of the conclusions derived from the empirical function $\hat{\sigma}_{GT,fit} = 109/A^{0.65}$, we have represented the ratio of the calculated and experimental unit cross-sections with fitted cross-section for Gamow-Teller transitions and are presented in Fig. 6 (b).

Consequently, to validate the theoretical calculations, one may compare them with outcomes from empirical relation where experimental data is unavailable. In Fig. 6 (a) it is clearly observed that the direct and total (D+E) contribution without tensor forces underestimate the empirical fitted data for low and high mass nuclei and overestimated the fitted data for medium mass nuclei. Furthermore, when we compute results after consideration of tensor forces with direct as well as total (D+E) terms contribution, it shows a reduction of magnitude with a factor of upto 3 except for ^{13}C nuclei (shows increase in magnitude with a factor of 2) along with the calculated results on excluding tensor forces.

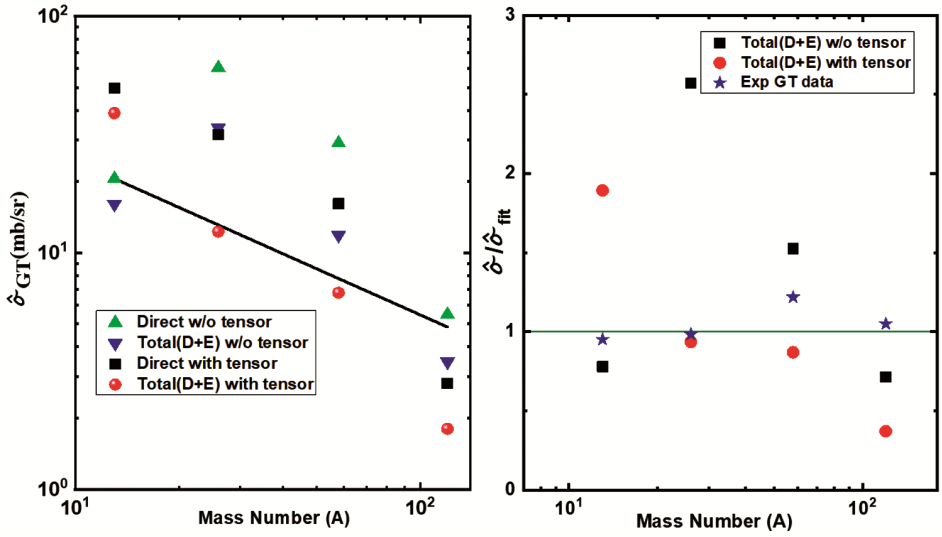

Fig. 6 — (Color online) The calculated unit cross-section for (^{3}He, t) Charge exchange reactions on targets ^{13}C, ^{26}Mg, ^{58}Ni and ^{120}Sn for GT transitions. (a) the up-triangles (green) and down-triangles (blue) shows direct (D) and total (D+E) calculations without considering tensor forces respectively. While solid (black) squares and solid (red) circles represents the results on consideration of tensor forces in the calculation with direct and total (D+E) terms respectively. The solid (black) line represents the unit cross-section obtained through fitted empirical function. (b) The ratio of the calculated Total (D+E) unit cross-section with fitted data shown by solid (black) square and solid (red) circle without and with tensor forces, respectively

Moreover, it is observed that the incorporating of tensor forces in the calculations bring the results towards the experimental fitted line for medium mass nuclei and away from the fitted data for low mass nuclei as well as for high mass nuclei. The reason for these discrepancies is the tensor component of the effective nucleon-nucleon interaction that mediates the charge-exchange reaction which may cause the interference between the $\Delta L = 2$, $\Delta S = 1$ amplitudes (mediated by the tensor-τ component of the interaction) and $\Delta L = 0$, $\Delta S = 1$ amplitudes (mediated by the $\sigma\tau$ component of the interaction) $\Delta L=0$ or 2 amplitudes since both contributes to the $\Delta J=1$ GT transition. The interference can be constructive as well as destructive.

4 Conclusion

We quantified the contribution of tensor forces in addition to knock-on exchange effects in (^{3}He, t) charge exchange reactions on different mass targets ^{13}C, ^{26}Mg, ^{58}Ni and ^{120}Sn at energy 140 MeV/nucleon using distorted wave impulse approximation (DWIA). Unit cross-section and angular distributions have been calculated with and without incorporation of contribution of exchange term and tensor forces. On inclusion of exchange term contribution significant quantitative variations in the magnitude of unit cross-section has been noticed (upto a factor of 3), which bring the predictions closer to empirically fitted data for medium mass nuclei. For ^{13}C (^{3}He, t) ^{13}N reaction, the inclusion of tensor forces with both direct and total contributions increased (arises due to constructive interference of tensor forces) the cross-section magnitude by 17% at small angles. Although, with the inclusion of tensor forces the cross-sections magnitude decreases for (^{3}He, t) reactions on ^{26}Mg, ^{58}Ni and ^{120}Sn targets and further indicating the destructive behaviour of tensor forces for these systems. In nutshell, the analysis of unit cross-sections signatures the significant influence of tensor forces in the analysis of charge-exchange reactions data.

References

1 Harakeh M N & Woude A V, Oxford University, New York, 2001.
2 Schulte A, Udagawa T, Osterfeld F & Cha D, *Phys Lett B*, 183 (1987) 243.
3 Taddeucci T N *et al*., *Nucl Phys A*, 469 (1987) 125.
4 Becchetti F D *et al*., *Nucl Phys A*, 271 (1976) 77.
5 Jaenecke J *et al*., *Nucl Phys A*, 526 (1991) 1.
6 Cappuzzello F *et al*., *Nucl Phys A*, 739 (2004) 30.
7 Cappuzzello F *et al*., *Prog Part Nucl Phys*, 128 (2023) 103999.
8 Li J J, Bertulani C A, Liu Y, Lou J L, Pang D Y, Sun X H, Yang B, Yang X F & Ye Y L, *Phys Rev C*, 102 (2020) 064601.
9 Fujita Y *et al*., *Phys Rev C*, 67 (2003) 064312.
10 Kim B T , Knobles D P, Stotts S A & Udagawa T, *Phys Rev C*, 61 (2000) 044611.

11 Diela F, Fujita Y, Fujita H, Cappuzzello F, Ganioglu E, Grewe E-W, Hashimoto T, Hatanaka K, Honma M & Itoh T, *Phys Rev C*, 99 (2019) 054322.
12 Fujita H, *et al*., *Phys Rev C*, 100 (2019) 034618.
13 Perdikakis G, Zegers R G T, Austin Sam M, Bazin D, Caesar C, Deaven J M, Gade A Galaviz, D, Grinyer G F, Guess C J, *et al*., *Phys Rev C*, 83 (2011) 054614.
14 Zegers R G T, Akimune H, Austin Sam M, Bazin D, Berg A M van den, Berg G P A, Brown, Alex B, Brown J, Cole A L, Daito I *et al*., *Phys Rev C*, 74 (2006) 024309.
15 Xu Z C, Zhang S, Li J G, Jin S L, Yuan Q, Cheng Z H, Michel N & Xu FR, *Phys Rev C*, 108 (2023) L031301.
16 Bai Sagawa C L, Zhang H Q, Zhang H, Coló X Z, Xu G, *FR Phys Rev Letts*, 83 (2011) 054316.
17 Bai Sagawa C L, Zhang H Q, Zhang H, Coló X Z, Xu G, *Phys Rev Letts*, 105 (2010) 072501.
18 Bai Sagawa C L, Zhang H, Zhang H Q, Coló X Z & Xu G, *Phys Letts B,* 675 (2009) 28.
19 Yang H M J, Bai Sagawa C L & Zhang H Q, *Phys Rev C*, 107 (2023) 014325.
20 Zegers R G T, Adachi T, Akimune H, Austin Sam M, van Den Berg A M, Brown B A, Fujita, Y, Fujiwara M, Gales S, Guess C J *et al*., *Phys Rev Letts,*. 99 (2007) 202501.
21 Fujita Y, Neveling R, Fujita H, Adachi T, Botha N T, Hatanaka K, Kaneda T, Matsubara H, Nakanishi K, Sakemi Y *et al*., *Phys Rev C,* 75 (2007) 057305.
22 Udagawa T, Schulte A, Osterfeld F, *Nucl Phys A*, 474 (1987) 131.
23 Riken, Nishina center for accelerator-based science, https://www.nishina.riken.jp/researcher/archive/program.
24 Singh P, *et al*., *Mod Phys Lett A,* 35 (2020) 2020045.
25 Ankita & Singh P, *Mod Phys Lett A,* 38 (2023) 2350066.
26 Love W G & Franey M A, *Phys Rev C,* 24 (1981) 1073.
27 Franey M A & Love W G, *Phys Rev C,* 31 (1985) 488.
28 Arndt R A, *et al*., *Phys Rev D*, 28 (1983) 1.
29 Fujimura H, Akimune H, Daito I, Fujiwara M, Hara K, Hara K Y, Harakeh M N, Ihara F Inomata T, Ishibashi K *et al*., *Phys Rev C*, 69 (2004) 064327.
30 Yamagata T, Utsunomiya H, Tanaka M, Nakayama S, Koori N, Tamii A, Fujita Y, Katori K, Inoue M, Fujiwara M *et al*., *Nucl Phys A*, 589 (1995) 425.
31 Van Der Werf S Y, Brandenburg S, Grasduk P, Sterrenburg W A, Harakeh M N, Greenfield M B, Brown B A & Fujiwara M, *Nucl Phys A*, 496, (1989) 305.
32 Chou W T, Warburton E K & Brown B, *Alex Phys Rev C*, 47 (1993) 163.
33 ENSDF, Evaluated nuclear structure data center, http://www.nndc.bnl.gov.
34 Brown Richter B A, *WA Phys Rev C*, 74 (2006) 034315.
35 Otsuka M H, Takaharu & Brown, Alex B & Mizusaki, *Takahiro Phys Rev C*, 69 (2004) 034335.
36 Douma Agodi C A, Akimune C, Alanssari H, Cappuzzello M, Carbone F, Cavallaro D, Coló M, Diel G, Ejiri F *et al*., *Eur Phys J A*, 56 (2020) 51.
37 Jassim K S, *Chin J Phys,* 51 (2013) 441.
38 Gao B, *et al*., *Phys Rev C*, 101 (2020) 014308.
39 Sullivan C, *et al*., *Phys Rev C*, 98 (2018) 015804.